




# Electrospun $Y^{3+}$ -modified $BaFe_{12}O_{19}$ hexaferrite-based nano-fibers with enhanced magnetic behavior for magnetic memory devices and permanent magnets

Indu Sharma<sup>1</sup>, Neha Thakur<sup>1</sup>, Munisha Mahajan<sup>2</sup>, Rohit Jasrotia<sup>3,\*</sup>, Gagan Anand<sup>4</sup>, R. Neffati<sup>5</sup>, A. Dahshan<sup>5</sup>, H. I. Elsaedy<sup>5</sup>, Pankaj Sharma<sup>6</sup>, and Gagan Kumar<sup>2,\*</sup> 

<sup>1</sup> Department of Physics, Career Point University, Hamirpur, Himachal Pradesh 176041, India

<sup>2</sup> Department of Physics, Chandigarh University, Chandigarh, India

<sup>3</sup> School of Physics and Materials Science, Shoolini University, Solan, Himachal Pradesh, India

<sup>4</sup> Applied Science Cluster, School of Engineering, University of Petroleum & Energy Studies, Dehradun, Uttarakhand 248001, India

<sup>5</sup> Department of Physics, Faculty of Science, King Khalid University, P.O. Box-9004, Abha, Saudi Arabia

<sup>6</sup> Applied Science Department, National Institute of Technical Teachers Training and Research, Chandigarh, India

**Received:** 27 June 2023

**Accepted:** 4 October 2023

**Published online:**

18 November 2023

© The Author(s), under exclusive licence to Springer Science+Business Media, LLC, part of Springer Nature, 2023

## ABSTRACT

The need to work on a low-dimensional and large specific surface is the modern need for the technology to serve scientific purposes. In this view, M-type Ba-based hexaferrite with rare earth doping has been synthesized in nano-fibrous form using the electrospinning method, by fixing the processing parameters such as voltage, flow rate, working distance, and differently concentrated doped hexaferrite, i.e.,  $BaY_xFe_{12-x}O_{19}$ , where  $x = 0, 0.3$ , and  $0.5$ . An examination for the structural, microstructural, and magnetic behavior with the help of the X-ray diffraction technique (XRD), Fourier transform infrared spectroscopy (FTIR), vibrating sample magnetometer (VSM), and field emission scanning electron microscopy (FESEM) has been performed. All doped and un-doped fiber samples have a hexagonal phase having space group named  $P63/mmc$  as established through XRD results. FTIR results also confirm the chemical structure and stretching vibrations between the metal–oxygen complexes of all the samples. FESEM results have revealed no apparent change in the fiber diameter with doping concentration. The fiber specimen having  $x = 0.3$  gives highest saturation and remnant magnetization of about 70.19 emu/g and 36.47 emu/g, correspondingly, followed by  $x = 0.0$ . Therefore, the fabricated materials with such excellent magnetic traits can become promising candidates in multifunctional applications, like recording media and the formation of permanent magnets.

Address correspondence to E-mail: rohitsinghjasrotia4444@gmail.com; physics.bhargava@gmail.com

## 1 Introduction

Because of the high coercivity ( $H_c$ ), barium hexaferrite ( $\text{BaFe}_{12}\text{O}_{19}$ ), the M-type hexaferrites, can generally be regarded as a hard magnetic matter [1]. These hexaferrites were employed in several technological fields, including high-density recording, telecommunication, magneto-optical recording, and permanent magnets [2, 3].  $\text{BaFe}_{12}\text{O}_{19}$  (BFO) also has poor electrical conductivity along with prominent values of dielectric constant at higher frequencies, making it suitable for the microwave circuit applications [1]. Furthermore, due to their useful traits (i.e., electrical, optical, structural, multiferroic), several hexaferrites with diamagnetically substituted Fe positions demonstrated the numerous intriguing practical uses [4–12]. Later, substituted hexaferrites with enhanced traits were also described in the literature [13–17] by replacing  $\text{Fe}^{3+}$  ions with various cations or combinations of cations at various crystallographic locations. Furthermore, barium hexaferrites replaced with diamagnetic cations have recently been found to have significant multiferroic traits and spontaneous polarization at ambient conditions. M-type hexaferrites fabricated using a modified ceramic synthesis method have magnetoelectric properties superior to well-known  $\text{BiFeO}_3$  (BFO) orthoferrite multiferroic at room temperature [18–23]. However, these materials may be prepared relatively easily due to environmental stability and affordable production costs. To demonstrate the microwave device applications, the hexaferrites exclusively implemented the higher cut-off frequencies as opposed to the spinel-structured ferrites [24]. Sol–gel auto-combustion [25, 26], sol–gel precursor coating [27, 28], wet milling [29], electrospinning [30], chemical co-precipitation [31], co-precipitation [32], sol–gel-aided electrospinning [33], carbon combustion [34], sonochemical method [35], as well as ball milling [36] are just a few of the recent synthesis methods that have been used to synthesize hexaferrite [37–41]. Although, as per best of the authors' understanding, most recent works concentrate on powders. The size and density of these hexagonal single-crystal ferrites limit their potential as microwave absorbers and shielding materials. Previous research has advocated the development of magnetic absorbing materials with smaller dimensions and greater specific surface areas to address this limitation and boost their absorbing capabilities per unit mass [42–44]. Fibers often have a substantially higher magnetic permeability than non-fibrous materials

of the same volume. Due to higher specific surface area, the M-type barium ferrite nano-fibers develops a decreased specific gravity. Its large specific surface area also aids in the absorption of electromagnetic radiation. Electrospinning is a state-of-the-art, highly efficient method for producing nano-fibers with high specific surface areas, porous architectures, and consistent diameters [45]. Given the strong connection between the chemical composition, ion arrangement within the crystal unit, and the electromagnetic features along with ferromagnetic resonance of pure BFO M-type ferrite, diverse ion doping approaches have been explored to customize these traits [46]. Because of decent electrical and magnetic traits of rare earth ions, including  $\text{La}^{3+}$ ,  $\text{Gd}^{3+}$ ,  $\text{Sm}^{3+}$ ,  $\text{Y}^{3+}$ ,  $\text{Pr}^{3+}$ ,  $\text{Ce}^{3+}$ ,  $\text{Bi}^{3+}$ , and  $\text{Ti}^{4+}$ , early study found that the magnetic behaviors of BFO may be modified by swapping  $\text{Ba}^{2+}/\text{Fe}^{3+}$  by these ions [47–50]. For instance, many researchers have used different methods to synthesize materials, such as  $\text{Ba}_{1-x}\text{La}_x\text{Fe}_{12}\text{O}_{19}$  [47, 48],  $\text{Ba}_{1-x}\text{Sm}_x\text{Fe}_{12}\text{O}_{19}$  [51],  $\text{BaBi}_x\text{La}_x\text{Y}_x\text{Fe}_{12-3x}\text{O}_{19}$  [52],  $\text{BaTi}_x\text{Fe}_{12-(4/3)x}\text{O}_{19}$  [49],  $\text{Ba}_{1-x}\text{Co}_x\text{Fe}_{12}\text{O}_{19}$  [53],  $\text{BaBi}_x\text{La}_x\text{Fe}_{12-2x}\text{O}_{19}$  [54], and  $\text{BaBi}_x\text{La}_x\text{Y}_x\text{Fe}_{12-3x}\text{O}_{19}$  [50].

By this point, much research has been carried out on the  $\text{BaFe}_{12}\text{O}_{19}$  hexaferrites' magnetic characteristics [55–58]. Several researchers have examined Ba hexaferrites with Y substitutions [50, 52, 59, 60]. However, no investigation on structural, morphological, and magnetic behavior of Electrospun nano-fibrous  $\text{BaY}_x\text{Fe}_{12-x}\text{O}_{19}$ , where  $x = 0.0, 0.3$ , and  $0.5$  hexaferrites is available in the literature. Therefore, here, we report a systematic study of electrospun  $\text{Y}^{3+}$ -doped BFO in nano-fiber form for the structural, magnetic, and morphological traits.

## 2 Experimental

### 2.1 Materials and methods

The sol of all the samples has been first prepared using the citrate precursor method to prepare nano-fibers. This sol has been mixed with PVP solution for forming  $\text{BaFe}_{12-x}\text{Y}_x\text{O}_{19}/\text{PVP}$ . Aqueous solutions of ferric nitrate nonahydrate ( $\text{Fe}(\text{NO}_3)_3 \cdot 9\text{H}_2\text{O}$ ), barium nitrate ( $\text{Ba}(\text{NO}_3)_2$ ), and yttrium acetate ( $\text{Y}(\text{CH}_3\text{COO})_3$ ) were prepared in deionized water (each with volume of 40 ml). Further, aqueous citric acid was prepared and aforementioned solutions were added on continuous stirring to  $\text{Ba}^{2+}$  and  $\text{Fe}^{3+}$  (citric acid to nitrate molar

ratio is 1:1). Later ammonium hydroxide was utilized to maintain pH level of around 7.0. The mixture was then set on a hot plate and cooked for 4 h at 60 °C. Eventually, the gelation occurred as the water evaporated. The gel was dissolved in a clear solution of polymer (22.5 wt%) comprising 3.0-g polyvinylpyrrolidone (PVP) for electrospinning. After 12 h of magnetic agitation, this liquid was transferred to a polypropylene capillary fitted through stainless steel spinneret. The spinneret was wired to the system's high-voltage source. The input power was kept at roughly 19.0 kV throughout the electrospinning process, and the separation between the collector and spinneret was optimized at 10.0 cm in order to accumulate the nano-fibers. Furthermore, the flow rate remained constant at 0.5 ml/hr throughout the process. After being retrieved, the  $\text{BaFe}_{12-x}\text{Y}_x\text{O}_{19}$ /PVP fibers were dried and then calcined at 650 °C for 2 h each to achieve the final  $\text{BaFe}_{12-x}\text{Y}_x\text{O}_{19}$  nano-fibers. The dried fibers were then characterized for their structural, morphological, and magnetic traits.

## 2.2 Characterization procedures

The XRD technique with  $\text{Cu-K}_\alpha$  source (MiniFlex II, Rigaku) has been used for structural analysis, and the FTIR study has been performed with an FTIR spectrophotometer. The morphology has been reported using FESEM (Carl Zeiss Supra 55 model). Furthermore, the VSM (EZ9, MicroSense model) has been utilized to analyze the magnetic behaviors.

## 3 Results and discussion

### 3.1 Structural study

XRD graphs for  $\text{BaFe}_{12-x}\text{Y}_x\text{O}_{19}$  nano-fibers with varied  $\text{Y}^{3+}$  ion contents and calcined at 650 °C for 2 h are given in Fig. 1. It is evident by XRD plots that  $\text{Y}^{3+}$  cations were well incorporated in  $\text{BaFe}_{12}\text{O}_{19}$  for every doping concentrations of  $\text{Y}^{3+}$  ions as all the peaks resembles well with the PDF No. 43-0002. The impurity peaks corresponding to secondary phases of  $\alpha\text{-Fe}_2\text{O}_3$  were observed when  $\text{Y}^{3+}$  ion content increased from 0.3 to 0.5.

For better understanding, the Rietveld refinement of hexaferrites having a hexagonal phase and space group  $P63/mmc$  was performed via Fullprof suite software. The refined patterns are given in Fig. 2. It has

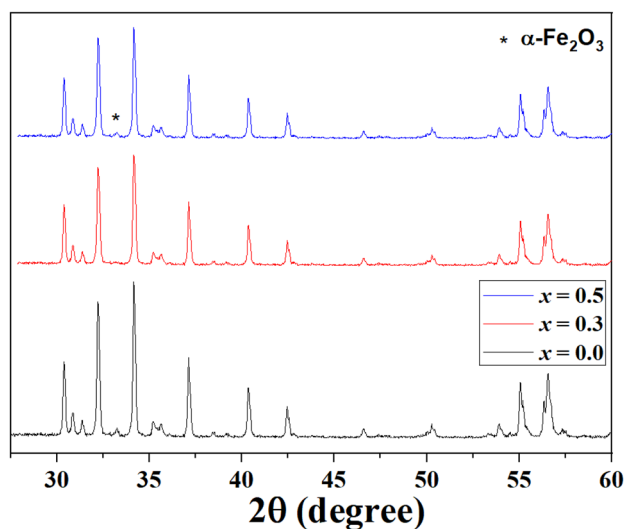


**Fig. 1** XRD patterns of prepared hexaferrite-based nano-fibers

been noted that for  $x = 0.3$ , all the peaks are assigned, which shows the absence of impurity phases. The lattice parameters ( $a$  &  $c$ ) and atomic positions are presented in Table 1 which represents the variation in “ $a$  and  $c$ .” The table shows that these parameters reduce with increasing concentration of  $\text{Y}^{3+}$ . R-weighted profile ( $R_{wp}$ ) and goodness of fit ( $\chi^2$ ) are also represented in Table 1. For all samples, the goodness of fit is approaching 1, which validates the excellent fitting results. This variation in cell volume and lattice parameters is a result of incorporation of  $\text{Y}^{3+}$  ions with different ionic radii onto  $\text{Fe}^{3+}$  lattice site causing lattice distortion. However, the ratio of  $c$  and  $a$  (i.e.,  $c/a$ ) is less than 3.98, which confirms the existence of hexagonal phase for all the produced hexaferrite-based fibers.

### 3.2 Morphology

A FESEM view of  $\text{BaFe}_{12-x}\text{Y}_x\text{O}_{19}$ /PVP (where  $x = 0.0, 0.30, 0.50$ ) nano-fibers is shown in Fig. 3. The fiber-like morphology is obtained as a result of the electrospinning synthesis. The cross-section of each nano-fiber has been observed to be uniformly smooth. The diameter of the fibers has been measured with the help of software named ImageJ. The random orientation of the continuous fiber was used to collect them and their average diameter was  $103 \pm 30$  nm,  $101 \pm 10$  nm, and  $102 \pm 10$  nm for  $x = 0.00, 0.3, \text{ and } 0.5$ , correspondingly. Therefore, no such variation has been observed in the diameter of the nano-fibers for doped and undoped samples. This may be due to the processing



**Table 1** Refined parameters of XRD data for prepared hexaferrite-based nano-fibers

| Sample             | $x=0.0$           | $x=0.3$           | $x=0.5$           |
|--------------------|-------------------|-------------------|-------------------|
| a (Å)              | 5.888             | 5.886             | 5.885             |
| c (Å)              | 23.189            | 23.184            | 23.182            |
| Ba                 | 0.66/0.33/0.25    | 0.66/0.33/0.25    | 0.66/0.33/0.25    |
| Fe1                | 0.0/0.0/0.0       | 0.0/0.0/0.0       | 0.0/0.0/0.0       |
| Fe2                | 0.0/0.0/0.259     | 0.0/0.0/0.260     | 0.0/0.0/0.260     |
| Fe3                | 0.33/0.66/0.0272  | 0.33/0.66/0.0268  | 0.33/0.66/0.0267  |
| Y4                 | –                 | 0.33/0.66/0.186   | 0.33/0.66/0.185   |
| Fe4                | 0.33/0.66/0.189   | 0.33/0.66/0.186   | 0.33/0.66/0.185   |
| Y5                 | –                 | 0.168/0.336/0.890 | 0.168/0.336/0.891 |
| Fe5                | 0.168/0.336/0.892 | 0.168/0.336/0.890 | 0.168/0.336/0.891 |
| OI                 | 0.0/0.0/0.151     | 0.0/0.0/0.150     | 0.0/0.0/0.150     |
| OII                | 0.33/0.66/0.943   | 0.33/0.66/0.943   | 0.33/0.66/0.942   |
| OIII               | 0.183/0.367/0.250 | 0.183/0.367/0.251 | 0.183/0.367/0.252 |
| OIV                | 0.156/0.312/0.052 | 0.156/0.312/0.050 | 0.156/0.312/0.051 |
| OV                 | 0.50/0.00/0.150   | 0.50/0.00/0.150   | 0.50/0.00/0.151   |
| V(Å <sup>3</sup> ) | 803.92            | 803.20            | 802.86            |
| R <sub>wp</sub>    | 31.4              | 30.1              | 28.6              |
| χ <sup>2</sup>     | 1.60              | 1.91              | 1.72              |

( $M_s$ ), giving the highest value of  $M_s$  for doping concentration of 0.03 (Table 2). The similar trend was observed for remnant magnetization ( $M_r$ ) as shown in Table 2.  $BaFe_{12}O_{19}$  structures have five different sites with varying distribution of  $Fe^{3+}$ , i.e., 3 octahedral, 1 trigonal-bipyramidal, and 1 tetrahedral site. The large cations of  $Ba^{2+}$  usually reside in oxygen lattice within unit cell [64, 65]. The fiber-like morphologies have noticeable impact on magnetic behaviors of the material. It has been already studied that M-type barium ferrite nano-fibers possess elevated specific surface area, contributing to reduced specific gravity and facilitating electromagnetic radiation absorption [45, 66].

Three of these octahedral sites in the crystal structure of  $Fe^{3+}$  correspond to spin-up states, while the other two correspond to spin-down states. The polar opposite spins are coupled together by  $O^{2-}$  ion exchange contact [64]. The magnetic moment of  $BaFe_{12}O_{19}$  is caused by  $Fe^{3+}$  ion, possessing a magnetic moment of  $5\mu_B$ . As a result,  $BaFe_{12}O_{19}$  achieve  $20\mu_B$  of net magnetic moment [54]. Non-magnetic  $Y^{3+}$  ions can theoretically fill spin-down sites within  $BaFe_{12}O_{19}$  by substitution. This results in fewer  $Fe^{3+}$

ions being in their spin-down state and more being in their spin-up state. The system's net magnetic moment increases as a result of the redistribution. As a result, when  $x=0.30$ , there is an increase in saturation magnetization and retentivity. Since  $Y^{3+}$  ions (non-magnetic) have already occupied the spin-down states, therefore any additional doping happens in the spin-up states. As a result, the saturation magnetization and retentivity drop and the net magnetic moment also decreases.

## 4 Conclusion

$BaY_xFe_{12-x}O_{19}$  (where  $x=0.0, 0.3, 0.5$ ) hexaferrite-based nano-fibers were synthesized using electrospinning synthesis route. The processing reaction parameters that play a crucial part in the generation of fibers in electrospinning were optimized at fixed values, such as flow rate = 0.5 ml/hr, input voltage 19 kV, and needle tip-to-collector distance = 10 cm. A hexagonal phase with some impurities has been observed in the XRD results for all the prepared nano-fibers. The prepared nano-fibers with  $101 \pm 10$  nm diameter shows ferrimagnetic phenomenon

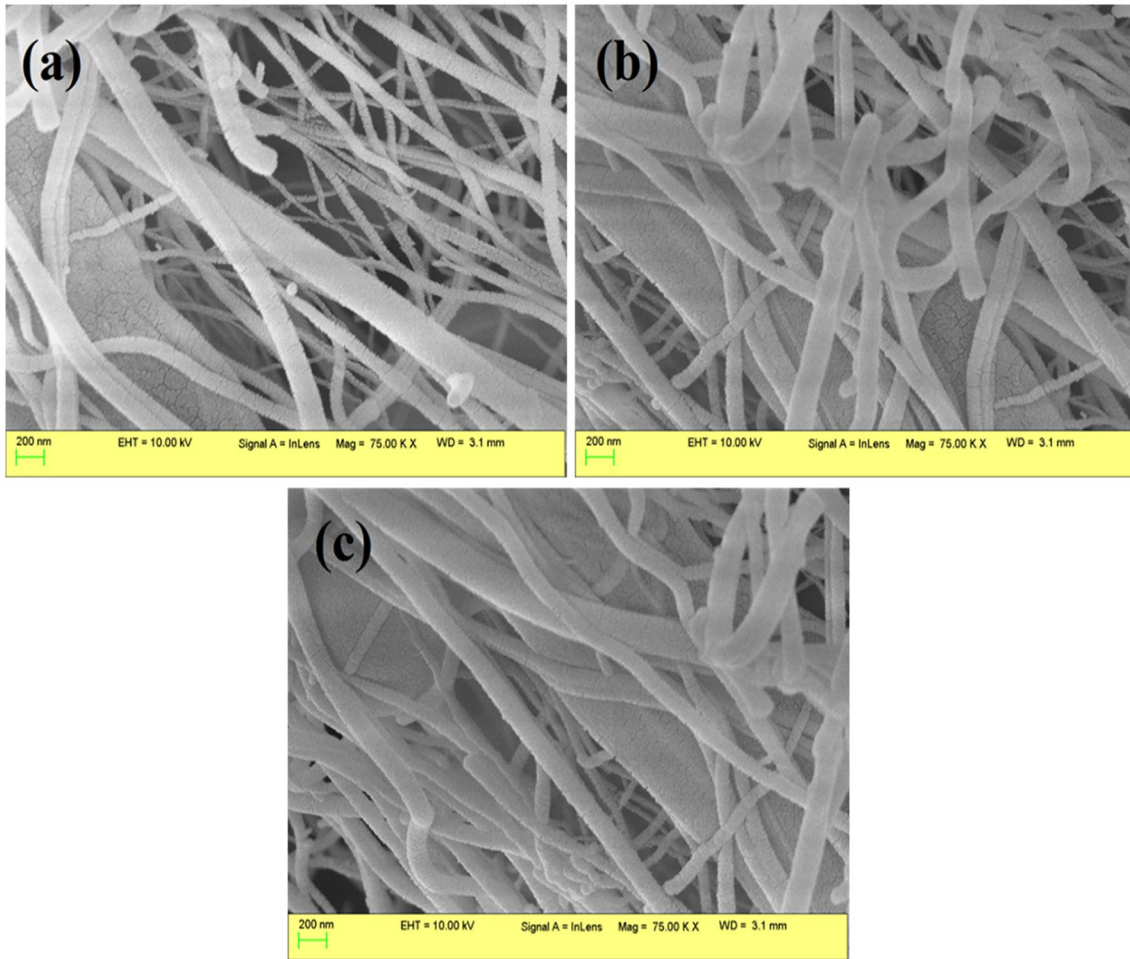


**Fig. 3** FESEM images for prepared hexaferrite-based nano-fibers

with maximum  $M_s$  and  $H_c$  of 70.19 emu/g and 36.47 Oe. The produced barium hexaferrite magnetic nanoparticles are dispersed over the nano-fibers, which therefore increases the surface area of the nanoparticles. This increased surface area elevated the strong magnetic interactions with the polymer matrix. This modifies the

physiochemical traits of prepared nano-fibers with an enhancement in the magnetic properties as compared to that of un-doped hexaferrite. The high magnetic nature of the doped BFO nano-fibers makes it beneficial in the development of magnetic memory, permanent magnets, and magnetic recording.

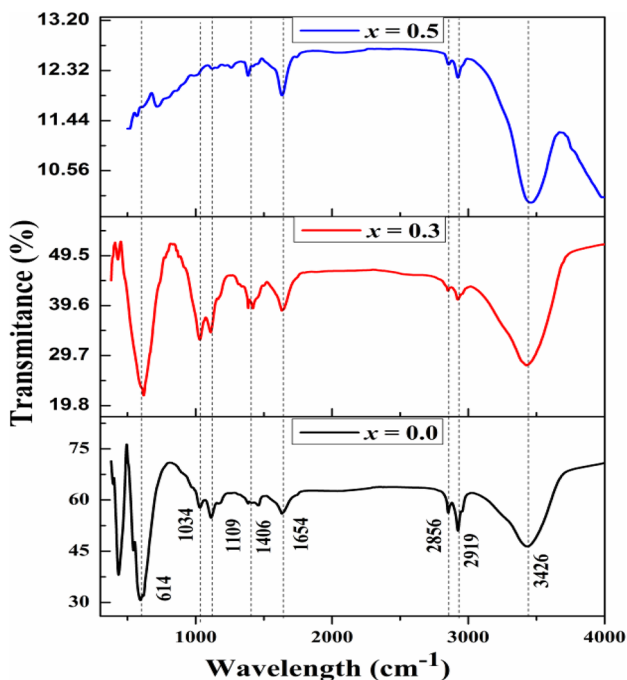


Fig. 4 FTIR spectra of prepared hexaferrite-based nano-fibers

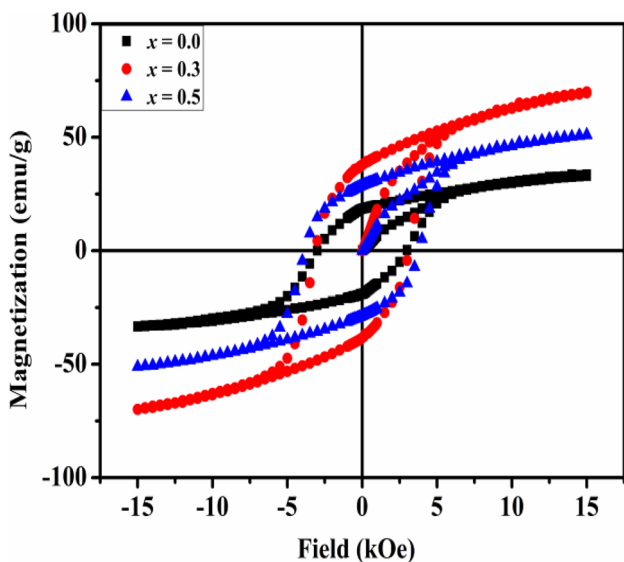


Fig. 5 The magnetization versus magnetic intensity pattern at ambient temperature for the prepared hexaferrite-based nano-fibers

**Table 2** Magnetic results for coercivity, retentivity, and saturation magnetization for hexaferrite-based nano-fibers

| $x$ | Saturation magnetization (emu/g) | Retentivity (emu/g) | Coercivity (kOe) |
|-----|----------------------------------|---------------------|------------------|
| 0.0 | 32.55                            | 17.91               | 2.77             |
| 0.3 | 70.19                            | 36.47               | 3.27             |
| 0.5 | 51.63                            | 27.70               | 3.90             |

### Acknowledgements

The authors extend their appreciation to the Deanship of Scientific Research at King Khalid University for funding this work through Large Groups Project under grant number RGP.2/151/44.

### Author contributions

IS, NT, and MM contributed to synthesis and characterizations. RJ, GA, and RN contributed to result analysis and writing. AD and HIE prepared and revised the manuscript, PS and GK contributed to final editing.

### Funding

The authors extend appreciation to the Deanship of Scientific Research at King Khalid University for funding this work through Large Groups Project under grant number (RGP.2/151/44).

### Data availability

All the relevant data are included in the article.

### Declarations

**Conflict of interest** The authors declare that they have no conflicts of interest.

**Ethical approval** None of the authors conducted studies involving human participants or animals for this article.

## References

- B.K. Rai, S.R. Mishra, V.V. Nguyen, J.P. Liu, J. Alloy. Compd. **550**, 198 (2013)
- N.V. Bharathi, P. Kavitha, S. Ramaswamy, S.S. Jayabalakrishnan, K. Sakthipandi, Bull. Mater. Sci. **45**, 172 (2022)
- V.P. Singh, R. Jasrotia, R. Kumar, P. Raizada, S. Thakur, K.M. Batoo, M. Singh, World J. Condens. Matter Phys. **8**, 36 (2018)
- D.A. Vinnik, I.A. Ustinova, A.B. Ustinov, S.A. Gudkova, D.A. Zherebtsov, E.A. Trofimov, N.S. Zabeivorota, G.G. Mikhailov, R. Niewa, Ceram. Int. **43**, 15800 (2017)
- D.S. Klygach, M.G. Vakhitov, D.A. Vinnik, A.V. Bezborodov, S.A. Gudkova, V.E. Zhivulin, D.A. Zherebtsov, C.P. SakthiDharan, S.V. Trukhanov, A.V. Trukhanov, A.Y. Starikov, J. Magn. Magn. Mater. **465**, 290 (2018)
- D.A. Vinnik, D.S. Klygach, V.E. Zhivulin, A.I. Malkin, M.G. Vakhitov, S.A. Gudkova, D.M. Galimov, D.A. Zherebtsov, E.A. Trofimov, N.S. Knyazev, V.V. Atuchin, S.V. Trukhanov, A.V. Trukhanov, J. Alloy. Compd. **755**, 177 (2018)
- D.A. Vinnik, S.A. Gudkova, R. Niewa, Mater. Sci. Forum **843**, 3 (2016)
- A.V. Trukhanov, S.V. Trukhanov, L.V. Panina, V.G. Kostishyn, D.N. Chitanov, I.S. Kazakevich, A.V. Trukhanov, V.A. Turchenko, M.M. Salem, Ceram. Int. **43**, 5635 (2017)
- S.V. Trukhanov, A.V. Trukhanov, V.A. Turchenko, A.V. Trukhanov, E.L. Trukhanova, D.I. Tishkevich, V.M. Ivanov, T.I. Zubar, M. Salem, V.G. Kostishyn, L.V. Panina, D.A. Vinnik, S.A. Gudkova, Ceram. Int. **44**, 290 (2018)
- S.V. Trukhanov, A.V. Trukhanov, V.A. Turchenko, A.V. Trukhanov, D.I. Tishkevich, E.L. Trukhanova, T.I. Zubar, D.V. Karpinsky, V.G. Kostishyn, L.V. Panina, D.A. Vinnik, S.A. Gudkova, E.A. Trofimov, P. Thakur, A. Thakur, Y. Yang, J. Magn. Magn. Mater. **457**, 83 (2018)
- V.A. Turchenko, S.V. Trukhanov, A.M. Balagurov, V.G. Kostishyn, A.V. Trukhanov, L.V. Panina, E.L. Trukhanova, J. Magn. Magn. Mater. **464**, 139 (2018)
- R. Jasrotia, V.P. Singh, R. Kumar, K. Singha, M. Chandel, M. Singh, Results Phys. **12**, 1933 (2019)
- A.V. Trukhanov, V.O. Turchenko, I.A. Bobrikov, S.V. Trukhanov, I.S. Kazakevich, A.M. Balagurov, J. Magn. Magn. Mater. **393**, 253 (2015)
- S.V. Trukhanov, A.V. Trukhanov, V.A. Turchenko, V.G. Kostishin, L.V. Panina, I.S. Kazakevich, A.M. Balagurov, J. Magn. Magn. Mater. **417**, 130 (2016)
- S.V. Trukhanov, A.V. Trukhanov, V.G. Kostishyn, L.V. Panina, V.A. Turchenko, I.S. Kazakevich, A.V. Trukhanov, E.L. Trukhanova, V.O. Natarov, A.M. Balagurov, J. Magn. Magn. Mater. **426**, 554 (2017)
- A.V. Trukhanov, S.V. Trukhanov, L.V. Panina, V.G. Kostishyn, I.S. Kazakevich, A.V. Trukhanov, E.L. Trukhanova, V.O. Natarov, V.A. Turchenko, M.M. Salem, A.M. Balagurov, J. Magn. Magn. Mater. **426**, 487 (2017)
- S.K. Godara, M.P. Kaur, V. Kaur, P.S. Malhi, M. Singh, S. Verma, R. Jasrotia, J. Ahmed, M.S. Tamboli, A.K. Sood, J. King Saud Univ. Sci. **34**, 101963 (2022)
- S.V. Trukhanov, A.V. Trukhanov, V.G. Kostishin, L.V. Panina, I.S. Kazakevich, V.A. Turchenko, V.V. Kochervinskii, JETP Lett. **103**, 100 (2016)
- A. Trukhanov, L. Panina, S. Trukhanov, V. Turchenko, M. Salem, Chin. Phys. B **25**, 016102 (2015)
- A.V. Trukhanov, S.V. Trukhanov, V.G. Kostishin, L.V. Panina, M.M. Salem, I.S. Kazakevich, V.A. Turchenko, V.V. Kochervinskii, D.A. Krivchenya, Phys. Solid State **59**, 737 (2017)
- M.A. Almessiere, Y. Slimani, H. Güngüneş, A. Baykal, S.V. Trukhanov, A.V. Trukhanov, Nanomaterials **9**, 1 (2019)
- K. Sakthipandi, E. Ahilandeswari, A.S. Afroze, M. Arunachalam, A. Hossain, P. Thamilmaran, Physica B **568**, 42 (2019)
- P. Dhiman, R. Jasrotia, D. Goyal, G.T. Mola, Hexagonal Ferrites, Synthesis, Properties and Their Applications, in *Ferrite: Nanostructures with Tunable Properties and Diverse Applications*, vol. 112, ed. by G. Sharma, A. Kumar, P. Dhiman (Materials Research Forum LLC, Millersville, 2021), p.336
- M. Javed Iqbal, M. Naeem Ashiq, I. Hussain Gul, J. Magn. Magn. Mater. **322**, 1720 (2010)
- S. Kanagesan, S. Jesurani, R. Velmurugan, C. Kumar, T. Kalaivani **4**, 8959 (2010)
- S. Asiri, S. Güner, A.D. Korkmaz, M. Amir, K.M. Batoo, M.A. Almessiere, H. Gungunes, H. Sözeri, A. Baykal, J. Magn. Magn. Mater. **451**, 463 (2018)
- B. Huang, C. Li, J. Wang, J. Magn. Magn. Mater. **335**, 28 (2013)
- Y. Li, Q. Wang, H. Yang, Curr. Appl. Phys. **9**, 1375 (2009)
- M.B. Kaynar, Ş. Özcan, S.I. Shah, Ceram. Int. **41**, 11257 (2015)
- C.J. Li, B.N. Huang, J.N. Wang, J. Mater. Sci. **48**, 1702 (2013)



31. J.L. Mattei, C.N. Le, A. Chevalier, A. Maalouf, N. Nutehou, P. Queffelec, V. Laur, J. Magn. Mater. **451**, 208 (2018)
32. Z. Mosleh, P. Kameli, M. Ranjbar, H. Salamati, Ceram. Int. **40**, 7279 (2014)
33. X. Shen, M. Liu, F. Song, X. Meng, J. Sol-Gel. Sci. Technol. **53**, 448 (2010)
34. K.S. Martirosyan, E. Galstyan, S.M. Hossain, Y.J. Wang, D. Litvinov, Mater. Sci. Eng. B: Solid-State Mater. Adv. Technol. **176**, 8 (2011)
35. E. Ahilandeswari, R.R. Kanna, K. Sakthipandi, Physica B **599**, 412425 (2020)
36. W.S. Castro, R.R. Corrêa, P.I.P. Filho, J.M.R. Mercury, A.A. Cabral, Ceram. Int. **41**, 241 (2015)
37. D.A. Vinnik, D.A. Zherebtsov, L.S. Mashkovtseva, Dokl. Phys. Chem. **449**, 39 (2013)
38. D.A. Vinnik, S.A. Gudkova, D.A. Zherebtsov, E.A. Trofimov, L.S. Mashkovtseva, A.V. Trukhanov, S.V. Trukhanov, S. Nemrava, B. Blaschkowski, R. Niewa, J. Magn. Mater. **470**, 97 (2019)
39. D.A. Vinnik, A.S. Chernukha, S.A. Gudkova, V.E. Zhivulin, E.A. Trofimov, A.Y. Tarasova, D.A. Zherebtsov, M. Kalandija, A.V. Trukhanov, S.V. Trukhanov, A.V. Senin, L.I. Isaenko, N.S. Perov, R. Niewa, J. Magn. Mater. **459**, 131 (2018)
40. R.R. Kanna, K. Sakthipandi, N. Lenin, E.J.J. Samuel, J. Mater. Sci.: Mater. Electron. **30**, 4473 (2019)
41. R. Jasrotia, J. Prakash, R. Verma, P. Thakur, A. Kandwal, F. Wan, A. Thakur, Phys. B: Condens. Matter **667**, 415202 (2023)
42. S.K. Nataraj, B.H. Kim, M. dela Cruz, J. Ferraris, T.M. Aminabhavi, K.S. Yang, Mater. Lett. **63**, 218 (2009)
43. C. Shao, H. Guan, Y. Liu, X. Li, X. Yang, J. Solid State Chem. **177**, 2628 (2004)
44. S.K. Godara, V. Kaur, R. Jasrotia, S. Thakur, V.P. Singh, J. Ahmed, S.M. Alshehri, B. Pandit, M. Singh, P. Kaur, J. Magn. Mater. **564**, 170049 (2022)
45. C.J. Li, J.N. Wang, Mater. Lett. **64**, 586 (2010)
46. J. Qiu, M. Gu, H. Shen, J. Magn. Mater. **295**, 263 (2005)
47. I.A. Auwal, S. Güner, H. Güngüneş, A. Baykal, Ceram. Int. **42**, 12995 (2016)
48. S. Verma, O.P. Pandey, A. Paesano, P. Sharma, Physica B **448**, 57 (2014)
49. M.A. Amer, T.M. Meaz, S.S. Attalah, A.I. Ghoneim, Mater. Sci. Semicond. Process. **40**, 374 (2015)
50. Y. Bakış, I.A. Auwal, B. Ünal, A. Baykal, Compos. B Eng. **99**, 248 (2016)
51. L. Wang, J. Zhang, Q. Zhang, N. Xu, J. Song, J. Magn. Mater. **377**, 362 (2015)
52. S. Güner, I.A. Auwal, A. Baykal, H. Sözeri, J. Magn. Mater. **416**, 261 (2016)
53. V.C. Chavan, S.E. Shirsath, M.L. Mane, R.H. Kadam, S.S. More, J. Magn. Mater. **398**, 32 (2016)
54. I.A. Auwal, A. Baykal, H. Güngüneş, S.E. Shirsath, Ceram. Int. **42**, 3380 (2016)
55. S. Dursun, R. Topkaya, N. Akdoan, S. Alkoy, Ceram. Int. **38**, 3801 (2012)
56. B. Unal, Z. Durmus, A. Baykal, M.S. Toprak, H. Sozeri, A. Bozkurt, J. Alloy. Compd. **509**, 8199 (2011)
57. K. Sadhana, K. Praveena, S. Matheppanavar, B. Angadi, Appl. Nanosci. **2**, 247 (2012)
58. A. Sharma, R. Jasrotia, N. Kumari, S. Kumar, A. Verma, S.K. Godara, J. Ahmed, S.M. Alshehri, A.M. Tamboli, S. Kalia, J. Magn. Mater. **564**, 170124 (2022)
59. I.A. Auwal, H. Güngüneş, S. Güner, S.E. Shirsath, M. Sertkol, A. Baykal, Mater. Res. Bull. **80**, 263 (2016)
60. Y. Bakış, I.A. Auwal, B. Ünal, A. Baykal, Ceram. Int. **42**, 11780 (2016)
61. M.J. Pourhosseini Asl, A. Ghasemi, G.R. Gordani, J. Supercond. Nov. Magn. **28**, 109 (2015)
62. M. Ghobeiti Hasab, S.A. Seyyed Ebrahimi, A. Badiçi, J. Eur. Ceram. Soc. **27**, 3637 (2007)
63. F.M.M. Pereira, C.A.R. Junior, M.R.P. Santos, R.S.T.M. Sohn, F.N.A. Freire, J.M. Sasaki, J.A.C. Paiva, A.S.B. Sombra, J. Mater. Sci.: Mater. Electron. **19**, 627 (2008)
64. M. Chandra Dimri, H. Khanduri, H. Kooskora, I. Heinmaa, E. Joon, R. Stern, J. Magn. Mater. **323**, 2210 (2011)
65. S. Ounnunkad, Solid State Commun. **138**, 472 (2006)
66. C. Cheng, J. Dai, W. Feng, Z. Li, X. Wen, Appl. Phys. A **126**, 1 (2020)

**Publisher's Note** Springer Nature remains neutral with regard to jurisdictional claims in published maps and institutional affiliations.

Springer Nature or its licensor (e.g. a society or other partner) holds exclusive rights to this article under a publishing agreement with the author(s) or other rightsholder(s); author self-archiving of the accepted manuscript version of this article is solely governed by the terms of such publishing agreement and applicable law.